ARTICLE

Leaching behavior of phosphorous compounds from sewage sludge ash based on quantitative X-ray diffraction analysis

Pinjing He[1,3] · Xiaotong Zhang[1,2] · Fan Lü[2,3] · Liming Shao[1,3] · Hua Zhang[1,2,3]

Abstract

Phosphorus (P) is an essential and limited resource. Incineration sewage sludge ash (ISSA) contains a high amount of P, which can be recovered using chemical leaching methods. However, the recovery ratio depends on the speciation of P and the leaching conditions. In this study, hydrochloric acid was used as a leaching agent, and the effects of the hydrochloric acid concentration, leaching time, temperature, and liquid–solid ratio on the P leaching ratio were investigated. Furthermore, the co-leaching of macro-metals Ca, Al, Fe, and Mg was analyzed. The results showed that P leached rapidly within 30 min, where the leaching rate reached more than 80% and then gradually stabilized. The leaching concentrations of Ca and Mg had a significant correlation (correlation coefficient $r^2 > 0.90$), and both were leached completely. Al and P had similar leaching patterns, where the leaching rates increased initially and then decreased with time at 0.2 mol/L HCl. According to X-ray diffraction analysis and Rietveld refinement, the P in ISSA was mainly present in the forms of $Mg_3Ca_3(PO_4)_4$ and $AlPO_4$. When leached using 0.2 mol/L HCl at 55 °C with a liquid-to-solid ratio of 20 L/kg, the $AlPO_4$ and $Fe_3(H_2O)_3(PO_4)_2$ in ISSA dissolved initially and then precipitated on the surface of the solid phase, thereby impeding further P leaching.

Keywords Sewage sludge ash · Acid leaching · Phosphorous speciation · Quantitative X-ray diffraction analysis · Rietveld refinement

Introduction

Phosphorus (P) is an essential element for all organisms [1]. According to the U.S. Geological Survey (USGS), 90% of the P consumed by industry throughout the world is used in agricultural fertilizers and the remainder P is mainly utilized in feed products and the chemical industry [2]. By 2050, the demand for P is predicted to increase by 50–100% due to global population growth and changes in diet [3]. In

✉ Hua Zhang
   zhanghua_tj@tongji.edu.cn

1   Institute of Waste Treatment and Reclamation, College of Environmental Science and Engineering, Tongji University, Shanghai 200092, China

2   State Key Laboratory of Pollution Control and Resource Reuse, Tongji University, Shanghai 200092, China

3   Shanghai Institute of Pollution Control and Ecological Security, Shanghai 200092, China

addition, the global P flow is one direction [4, 5] and it can, no longer, be recovered after entering rivers or seas. Phosphate rock is the main source of P and, maybe, be exhausted as soon as within 100 years [3, 4, 6]. Thus, it is important to explore alternatives to phosphate rock and economically viable P-rich resources.

In the process of sewage treatment, 90% of P is fixed in the sewage sludge [7]. However, a serious ecological risk is associated with the direct recycling of P-containing sludge to farmland due to the presence of heavy metals, pathogens, and other hazardous components of the sludge [8, 9]. Incineration can achieve the maximal reduction and decontamination of sludge [10, 11], and 75–98% of the P in sewage sludge will remain in the incineration sewage sludge ash (ISSA) [12]. Studies indicated that P content (10–25% as P_2O_5) of ISSA is typically high [13, 14]. Therefore, ISSA is attractive as a raw material for P recovery in terms of its physical composition and particle morphological structure.

In terms of the dissolution–precipitation and complexation characteristics of P in ISSA, previous studies have investigated the effects of various leaching agents (such as organic acids, inorganic acids, chelating agents, and alkalis)

at different concentrations as well as the leaching temperature, leaching time, liquid-to-solid (L/S) ratio, and pH on the P leaching ratio [8, 15, 16]. The study showed that inorganic acids have the highest P leaching ratio [17], and that the ratio increases to equilibrium as the temperature, leaching agent concentration, and L/S ratio increase [18]. The chelating agent EDTA can be used as a pre-treatment agent to remove trace elements before P leaching [15]. At pH = 3–4, the dissolution of Ca-P compounds is accompanied by the precipitation of Fe–P and Al–P compounds, which hinder the continuous leaching of P [19]. The thermodynamic and kinetic properties as well as the factors that influence sludge leaching [20] have been investigated, which facilitate the recovery of P for use as chemical P fertilizers (Ca–P) [21], struvite [22, 23], phosphoric acid [24], etc. by the methods such as precipitation, adsorption, electrodialysis, and so on [21, 25, 26]. However, impurities such as metals and heavy metals in ISSA can dissolve in the extraction process and then precipitate during recovery processes to reduce the P recovery rate, product purity, and bioavailability [13, 27], thereby limiting the commercialization of P recovery products.

ISSA contains a variety of P-containing compounds and these different forms of P-containing compounds differ in terms of their recovery potentials, bioavailability, and leaching effects [28, 29]. To further improve the P recovery rate and quality of P-containing products, it is necessary to quantitatively analyze the speciation and mass distribution of P-containing compounds in ISSA, their changes during the leaching process and the associated mechanisms, and the specific chemical structure of P recovery products. Most previous studies employed X-ray diffraction (XRD), attenuated total reflection Flourier transformed infrared spectroscopy (ATR-FTIR), and scanning electron microscopy-energy dispersive X-ray spectroscopy (SEM–EDX) to qualitatively analyze the main types of P-containing compounds, as well as the combinations of P with Ca, Al, and Fe in ISSA, solid residues, and recovery products [17, 18]. The forms of P-containing compounds were estimated in sequential chemical extraction procedures or based on the leaching correlations among P and other elements [14]. However, a few studies have quantitatively investigated the morphological changes in different P-containing compounds in ISSA to elucidate the recovery mechanism.

XRD is an effective method for determining the mineralogical structure of multiphase solid samples. The Rietveld refinement method can effectively solve the overlapping problem for the diffraction peaks of various phases and calculate the absolute abundances of crystalline and amorphous phases in a sample when combination with an internal standard [30, 31]. The present study investigated the co-leaching and precipitation of P and elements such as Ca, Al, Fe, and Mg under different leaching conditions, and the controlling factors that affected the P leaching process were estimated based on the leaching kinetics and thermodynamics. XRD, the Rietveld refinement method, and SEM–EDX were combined to elucidate the chemical transformation and variations in the contents of P-containing compounds during acid leaching. The finding obtained in this study provide theoretical guidance to optimize the selectivity of P leaching processes and the preparation of P recovery products.

Materials and methods

Samples collection and treatments

The ISSA and dewatered sludge sample used in this study were collected from a sewage sludge incineration plant in Shanghai. The dewatered sludge was dried and then burned in a fluidized bed incinerator. The temperature in the combustion zone was controlled to above 850 °C. A schematic diagram illustrating the sludge incineration process is shown as Fig. S1. The flue gas was cleaned by the electrostatic precipitator and bag filter to remove particulate pollutants after adding lime and activated carbon. The bag filter ash was sampled as ISSA for use in the experiment.

Phosphorus leaching

Hydrochloric acid (GR, Sinopharm Chemical Reagent Co., Ltd, China) was used as the leaching agent, and the weight of ISSA sample for leaching was kept constant as 2.25 g. The leaching experiment was conducted in an incubator (BPH-9272, Bluepard, China) for a certain time with rotation at 55 rpm, after which the leaching mixtures were filtered through membranes with a pore size of 0.45 μm to separate the solid residues [7]. The detailed experimental conditions (HCl concentration, leaching time, L/S ratio, and temperature) are summarized in Table 1, and all of the experiments are conducted in triplicate ($n = 3$). The pH values of the

Table 1 Phosphorus leaching conditions for the ISSA

Factors	HCl concentration (mol/L)	Leaching time (min)	Temperature (°C)	L/S ratio (L/kg)
HCl concentration and leaching time	0.2, 0.3, 0.4, 0.5	5, 15, 30, 60, 120	20, 55	20:1
Temperature and leaching time	0.5	5, 15, 30, 60, 120	20, 30, 45, 55	20:1
L/S ratio and temperature	0.5	60	20, 55	5:1, 10:1, 20:1

filtrates were measured immediately and the elemental concentrations were then analyzed by inductively coupled plasma optical emission spectrometry (ICP-OES, 720ES, Agilent, USA). The P leaching ratio (E_P) is calculated as the percentage of the leached P amount to its original amount in the ISSA (Eq. 1):

$$E_P = \frac{C \cdot V}{a \cdot m} \times 100 \tag{1}$$

where E_P is the P leaching ratio, %; C represents P concentration in the leachate, mg/L; V is the volume of the leachate, L; a is the P content in the ISSA, mg/g; and m is the mass of the ISSA used in the leaching, g.

Solid-phase analysis

X-ray fluorescence (XRF, UniQuant, Thermo, USA) was used to determine the elemental contents of the dewatered sludge and ISSA samples after drying at 105 °C for 24 h. ISSA was digested using HCl-HNO$_3$-HF-HClO$_4$ [32] before ICP-OES analysis to obtain the P and metal contents according to the standard BS EN 13657:2002.

The solid residues obtained from leaching were dried at 105 °C for 24 h, and then ground and sieved to less than 150 μm. XRD (D8Advance, Bruker, Germany) was conducted (40 mA, 40 kV) to determine the mineralogical composition of the ISSA and solid residues. The qualitative analysis conditions for the crystalline phase were: step size = 0.02° and scan speed = 0.4 s/step. The quantitative analysis conditions for the crystalline and amorphous phases were: addition of 10% chromic oxide (Cr$_2$O$_3$, purity ≥ 99.0%) as an internal standard, step size = 0.01°, and scan speed = 1 s/step. SEM–EDX (PhenomProX, Phenom-World, The Netherlands) was performed to observe the surface micromorphology of the ISSA and solid residues.

Data analysis

Analysis of variance and correlation were conducted using Microsoft Excel 2016 and IBM Statistics 21 software to detect significant differences according to the various leaching conditions (HCl concentration, leaching temperature, leaching time, and L/S ratio) and the correlations between parallel sample results. The XRD patterns were analyzed using the MDI Jade 6 software to qualitatively determine the crystalline phases. GSAS software was used to fit the XRD patterns based on the Rietveld refinement method and to calculate the absolute contents of the crystalline phases and amorphous phases in the ISSA and solid residue according to Eqs. 2 and 3 [33]. Visual Minteq 3.1 was used to simulate the chemical equilibrium relationships between P (PO$_4^{3-}$) and macro-metals (Ca, Mg, Fe, and Al):

$$X_i = \frac{1}{1 - X_s}\left[\left(\frac{X_s}{X_{sc}}\right)X_{ic}\right] \tag{2}$$

$$X_a = \frac{1}{1 - X_s}\left[1 - \left(\frac{X_s}{X_{sc}}\right)\right], \tag{3}$$

where X_i is the actual content of the crystalline phase i, %; X_s is the actual content of the internal standard, %; X_{sc} is the calculated content of the internal standard determined using the Rietveld refinement method, %; X_{ic} is the calculated content of the crystalline phase i determined using the Rietveld refinement method, %; and X_a is the actual content of the amorphous phase, %.

Results and discussion

ISSA composition

Table 2 shows the elemental compositions of the dewatered sludge and ISSA, where the result indicates that Si, Al, P, Ca, Fe, Mg, and Na were the dominant elements in ISSA. The high Al content was due to the addition of Al salt during the flocculation and precipitation process in the wastewater treatment plant. Ca was mainly derived from the lime added in the flue gas treatment process [34]. The Zn content was 2.5–4.0 times higher than the Cu and Mn contents, which is basically consistent with the heavy metal distribution ratio found in dewatered sludge. The contents of Na, P, Al, and Mg in ISSA determined by XRF were higher compared with those obtained by ICP-OES after acid digestion. Similar findings were reported by Hoffmann et al. [35] and Wang et al. [22] who attributed the difference to the lack of calibration standards for the solid samples. The contents of Fe, Ca, Zn, Cu, Mn, and K obtained by XRF and ICP-OES are similar. Thus, the results obtained by XRF in this study are only considered suitable for reference purposes.

Figure S2 shows the qualitative XRD results obtained for ISSA. SiO$_2$ (quartz), Mg$_3$Ca$_3$(PO$_4$)$_4$ (Stanfieldite), CaAl$_2$Si$_2$O$_8$ (Anorthite), AlPO$_4$, Ca$_{2.7}$Mg$_{0.29}$(PO$_4$)$_2$ (Whitlockite), and Fe$_2$O$_3$ (Hematite) were the major crystal phases in ISSA, as also found in the other studies [22, 24].

Leaching characteristics of ISSA

Effects of acid concentration on P leaching ratio

The changes in the P leaching ratio (L/S = 20 L/kg) with time were studied at different acid concentrations under at 20 °C and 55 °C. As shown in Fig. 1, the P leaching ratio was affected significantly (p value = 0.00048 < 0.01) by the temperature when leaching using 0.2 mol/L hydrochloric

Table 2 Elemental composition of the dewatered sludge and ISSA (%)

Samples	Test method	Na	Si	P	Al	Fe	Mg	Ca	Zn	Cu	Mn	Pb	K
Dewatered sludge	XRF	0.31	4.15	1.33	1.54	1.55	0.46	1.21	0.062	0.017	0.017	0.01	0.75
ISSA	XRF	1.18	23.9	8.09	10.6	5.64	4.43	5.67	0.216	0.086	0.062	ND	3.01
	ICP-OES	0.68±0.02	ND	5.21±0.41	7.12±0.16	5.49±0.21	2.73±0.06	5.39±0.11	0.274±0.004	0.086±0.005	0.069±0.005	0.040±0.003	3.07±1.16

ND not detected

acid (the theoretical acid demand is calculated based on the molar ratio as $PO_4^{3-}:H^+ = 1:3$ [24]). The P leaching ratio was maintained as 57% at 20 °C, which was 50.4% lower than that at 55 °C for 30 min. Interestingly, the P leaching ratio decreased gradually with time at 55 °C and reached the lowest value after 120 min, which was 25% lower than that after leaching for 15 min. Other studies [8, 26] also obtained similar results. This difference may be attributed to P-bearing compounds dissolving initially and then adsorbing onto metal oxides in the solid residue (iron oxide, etc.), or the dissolved P could have crystallized or precipitated to form insoluble P-bearing compounds such as iron phosphate. As the HCl concentration increased, the effect of temperature on the P leaching ratio was no longer significant. By contrast, the HCl concentration significantly affected (p value = 0.0003 < 0.01) the P leaching ratio. Sufficient H^+ ions were present in the solution when the HCl concentration was 0.3 mol/L or higher and the P leaching ratio increased with time until it reached a plateau. At 30 min, nearly 90% of the P was leached from ISSA and the equilibrium was attained at about 60 min, which can be attributed to the acid-soluble nature of the P-bearing compounds in ISSA and the small particle size [18]. In some cases, the P leaching ratio was close to or greater than 100%, probably because the phosphorus contents in ISSA were underestimated by ICP-OES analysis after digestion [36].

Effects of temperature on P leaching ratio

For solid–liquid heterogeneous reactions, increasing the temperature is one of the most effective methods for enhancing the reaction rate. Figure 2 shows the effect of temperature on the P leaching ratio using 0.5 mol/L hydrochloric acid at L/S = 20 L/kg. The temperature and reaction time had significant effects on the P leaching ratio (p value = 1.24×10^{-14} and p value = 0.0014, respectively). As the temperature increased, the viscosity of the solution decreased, whereas the molecular motion strengthened intensely, thereby greatly enhancing the probability of the solid and solution coming into contact to enhance the P leaching ratio [37]. Leaching for 15 min and 30 min, the H^+ concentration was sufficient, and as the temperature increased, the increment of the P leaching ratio became insignificant, and thus, the values were similar at 45 °C and 55 °C. After 30 min, due to the consumption of H^+, the P leaching ratio increased in proportion to the increase in temperature.

Effects of L/S ratio on P leaching ratio

Figure 3 shows that L/S had a significant effect ($p = 0.003$) on the P leaching ratio. As L/S increased from 5 to 10 L/kg, the P leaching ratio increased by 1–1.6 times, but further increasing L/S to 20 L/kg changed the P leaching ratio only

Fig. 1 Effects of hydrochloric acid concentration on the P leaching ratio (L/S = 20 L/kg)
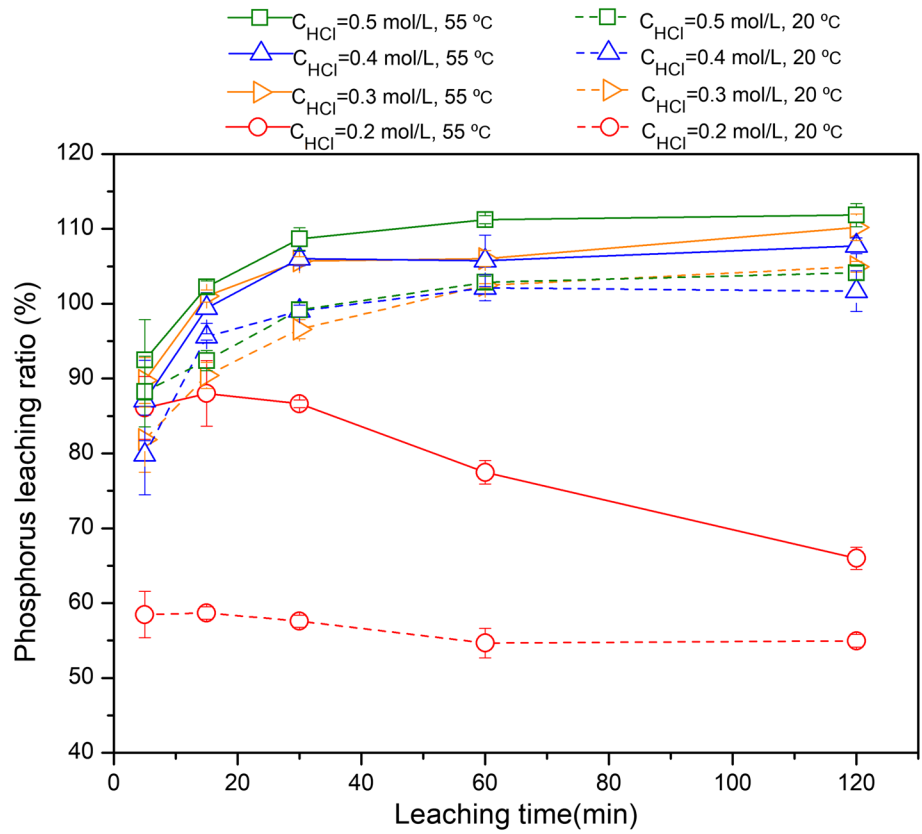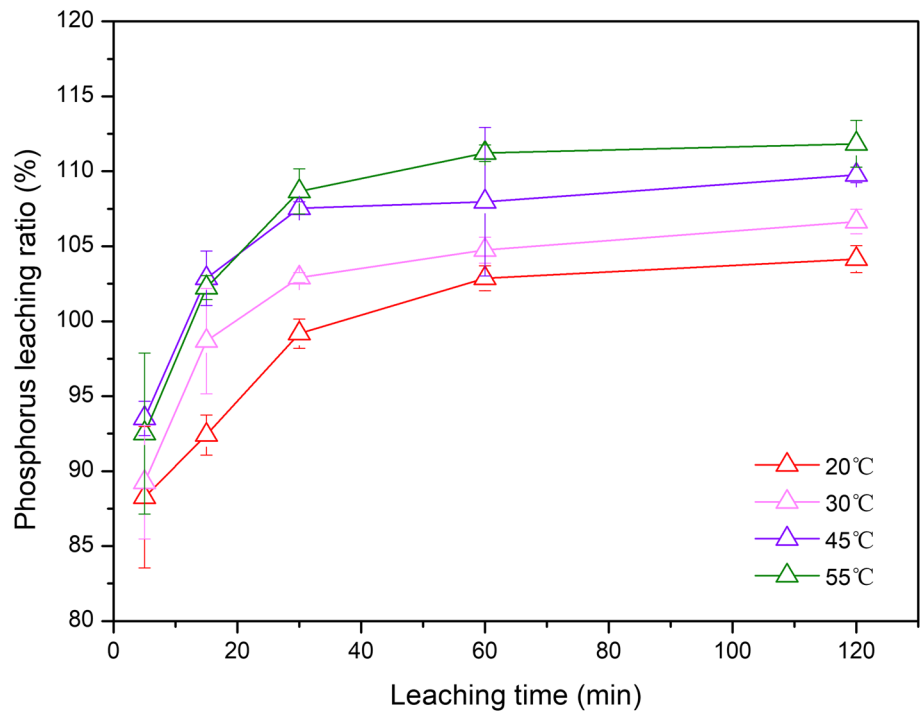

Fig. 2 Effects of temperature on P leaching ratio (0.5 mol/L HCl, L/S = 20 L/kg)

slightly. The two-tailed t-test results showed that the difference in the P leaching ratio at 55 °C for L/S = 10 L/kg and 20 L/kg was significant (t statistic = − 4.66 < −t critical = − 4.30, p value = 0.04), but not significant at 20 °C (t statistic = − 2.48 > −t critical = − 3.18, p value = 0.09). When L/S was relatively low, the P leaching ratio was negatively

Fig. 3 Effects of L/S ratio on P leaching ratio (0.5 mol/L HCl, leaching time 60 min)
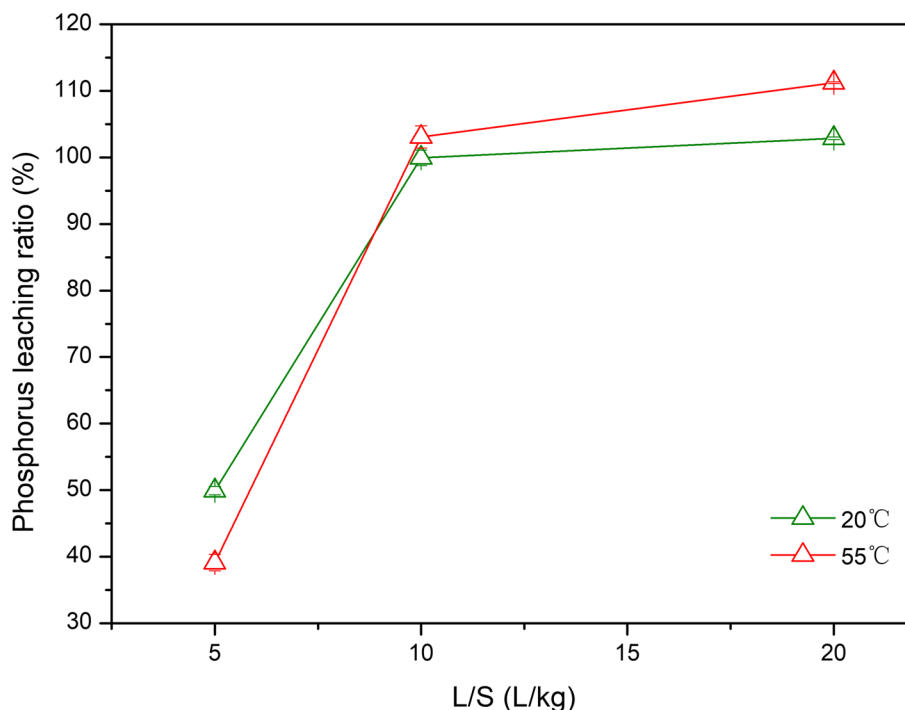
affected by the insufficient availability of HCl and the weak mass transfer efficiency between the solid and liquid phases [38, 39]. Increasing L/S is advantageous for improving the dispersion of the solid in the solution to enhance the mixing and obtain a high P leaching ratio. However, an excessive L/S will increase the cost of the reagent as well as increasing the cost of concentrating the P leachate [24, 40]. Therefore, to achieve a higher P leaching ratio and maintain low costs, L/S is preferably 10 L/kg.

Phosphorus leaching kinetics and thermodynamics

Acid leaching from ISSA is a complex solid–liquid heterogeneous mixing process that involves chemical reactions such as dissolution, precipitation, and other phenomena such as diffusion and infiltration. As shown in Fig. 1, the phosphorus leaching rate was high for the first 30 min, but it then decreased gradually, and the leaching rate even became negative when the acid concentration was 0.2 mol/L. Thus, it indicates that the leaching kinetic controlling factors changed as the reaction continued. In the early stage, phosphorus leaching was fast under the control of the chemical reaction and the diffusion resistance could be ignored. As the ISSA continued to dissolve, solid product layers were generated, where phosphorus-containing compounds precipitated or adsorbed on the surface of the ISSA, which increased the diffusion resistance [41] and hindered the further diffusion and permeation of H^+ ions, thereby confirming the appearance of a self-impeding effect [42, 43]. Therefore, according to the occurrence of

this phenomenon, the Drozdov equation (Eq. 4) including a self-impeding factor was employed to simulate the phosphorus leaching process from ISSA:

$$\frac{1}{t} \ln \frac{1}{1-x/100} - \beta_x \frac{\frac{x}{100}}{t} = k_m, \qquad (4)$$

where k_m is the rate constant, min^{-1}; β_x is the impeding coefficient, non-dimensional; t is the leaching time, min; and x is the phosphorus leaching efficient, %.

The simulation results are shown in Fig. S3 and S4. The intercepts and slopes of the fitted curves corresponding to k_m and β_x, respectively, are shown in Table 3.

As shown in Table 3, the rate constant k_m and the impeding coefficient β_x increased as the temperature increased at the same acid concentration. In addition, the impeding coefficient β_x increased as the acid concentration increased at the same temperature. When the acid concentration was 0.2 mol/L, the change in β_x was more obvious as the temperature increased, thereby indicating that the impeding effect of the solid product layers was more significant when insufficient H^+ ions were present. The correlation coefficients r^2 all exceeded 0.99, and thus, the fits were satisfactory. Compared with the kinetic equation that only considers the overall reaction controlling factor, the Drozdov equation includes a self-impeding factor and it can obtain better descriptions of the kinetic behavior of the phosphorus leaching process from ISSA.

Using the Arrhenius equation (Eq. 5), the activation energy at 0.5 mol/L HCl was calculated by simple linear

Table 3 Fitting results obtained using the Drozdov equation

Temperature (°C)	HCl concentration (mol/L)	Rate constant k_m (min^{-1})	Impeding coefficient β_x (non-dimensional)	Correlation coefficient r^2 (non-dimensional)
20	0.2	− 0.0002	1.3730	1.0000
20	0.3	0.0114	1.5902	0.9931
20	0.4	0.0090	1.6234	0.9991
20	0.5	0.0070	1.7642	0.9996
30	0.5	0.0107	1.7777	0.9975
45	0.5	0.0137	1.8746	0.9962
55	0.2	− 0.0006	1.7704	0.9998
55	0.3	0.0142	1.7117	0.9940
55	0.4	0.0138	1.7750	0.9956
55	0.5	0.0170	1.8224	0.9962

regression based on the reciprocal of the temperature ($\frac{1}{T}$) and rate constant:

$$\ln k_m = \ln A - \frac{E_A}{RT}, \tag{5}$$

where k_m is the rate constant, min^{-1}; A is the pre-exponential factor, min^{-1}; E_A is the apparent activation energy, kJ/mol; T is the temperature, K; and R is the molar gas constant, 8.314×10^{-3} kJ/(mol K). The fitted plot is presented in Fig. S5.

As shown in Fig. S5, the plot fitted well, with a correlation coefficient of 0.9665. According to Eq. 4, the activation energy was calculated as 19.26 kJ/mol. The magnitude of the activation energy can characterize the reaction rate, and thus, it can be used as an important parameter to analyze the factors responsible for controlling heterogeneous reactions to some extent. In general, the activation energy of a diffusion-controlled reaction is relatively small, ranging from 4 to 13 kJ/mol, whereas that for chemical reaction control is usually greater than 45 kJ/mol [44, 45]. The activation energy determined in this study was between these two values, thereby indicating that the acid leaching process from ISSA was controlled by a mixture of factors comprising chemical reaction and diffusion.

Macro-metal leaching

Figure 4 shows the effects of the acid concentration and leaching time on the concentrations of the macro-metals leached from ISSA. Due to the insolubility of iron oxides, the leaching concentration of Fe was basically maintained at 3.5–7.5 mmol/L, although it decreased slightly with time at 0.2 mol/L HCl. The leaching pattern for Al was similar to that for P, i.e., when the hydrochloric acid concentration (0.2 mol/L) was lower than the theoretical acid concentration, the leached concentration of Al increased initially and then decreased with time, and the effect of temperature was

highly significant on Al leaching. By contrast, when the hydrochloric acid concentration was greater than the theoretical requirement, the leached concentration of Al increased over time until it reached a constant value. With different acid concentrations, the leached concentrations of Ca and Mg were basically stable over time and the leaching patterns were similar. The Pearson's correlation coefficients indicated that the changes in the leached concentrations of Ca and Mg had a significant correlation (correlation coefficient $r^2 > 0.90$ for each leaching condition). In addition, the molar ratio of leached Ca relative to leached Mg was stable at between 1.4 and 1.5, and the leaching ratios both exceeded 70%. Based on the phase analysis results for ISSA shown in Fig. S2, elemental Ca and Mg mainly combined in the forms of $Ca_3Mg_3(PO_4)_4$ (Stanfieldite) and $Ca_{2.7}Mg_{0.29}(PO4)_2$ (Whitlockite). Due to the acid-soluble properties of Stanfieldite and Whitlockite [24], P combined with Ca and Mg dissolved preferentially. However, at 0.2 mol/L HCl, the P leaching ratio decreased, possibly because P combined with Al and Fe as a precipitate according to the leaching patterns for Al and Fe and the presence of the $AlPO_4$ and $Fe_3(H_2O)_3(PO_4)_2$ phases.

Principal component analysis has been conducted using the RStudio, to analyze the importance of factors (HCl concentration, leaching time, temperature, and L/S ratio) and the correlations of variables (the leaching ratios of P, Ca, Mg, Fe, and Al). As shown in Fig. S6, HCl concentration and L/S are the two principal factors. HCl concentration had a positive correlation to the P, Fe, and Al leaching, while L/S ratio showed more important role in Ca and Mg leaching. P, Al, and Fe leaching ratios have similar varying trends, whereas Ca and Mg, with high solubility, are relatively different.

Speciation transformation during leaching

Transformation of P-containing compounds

Qualitative analysis of crystal phase composition The chemical compositions of the raw ISSA and solid resi-
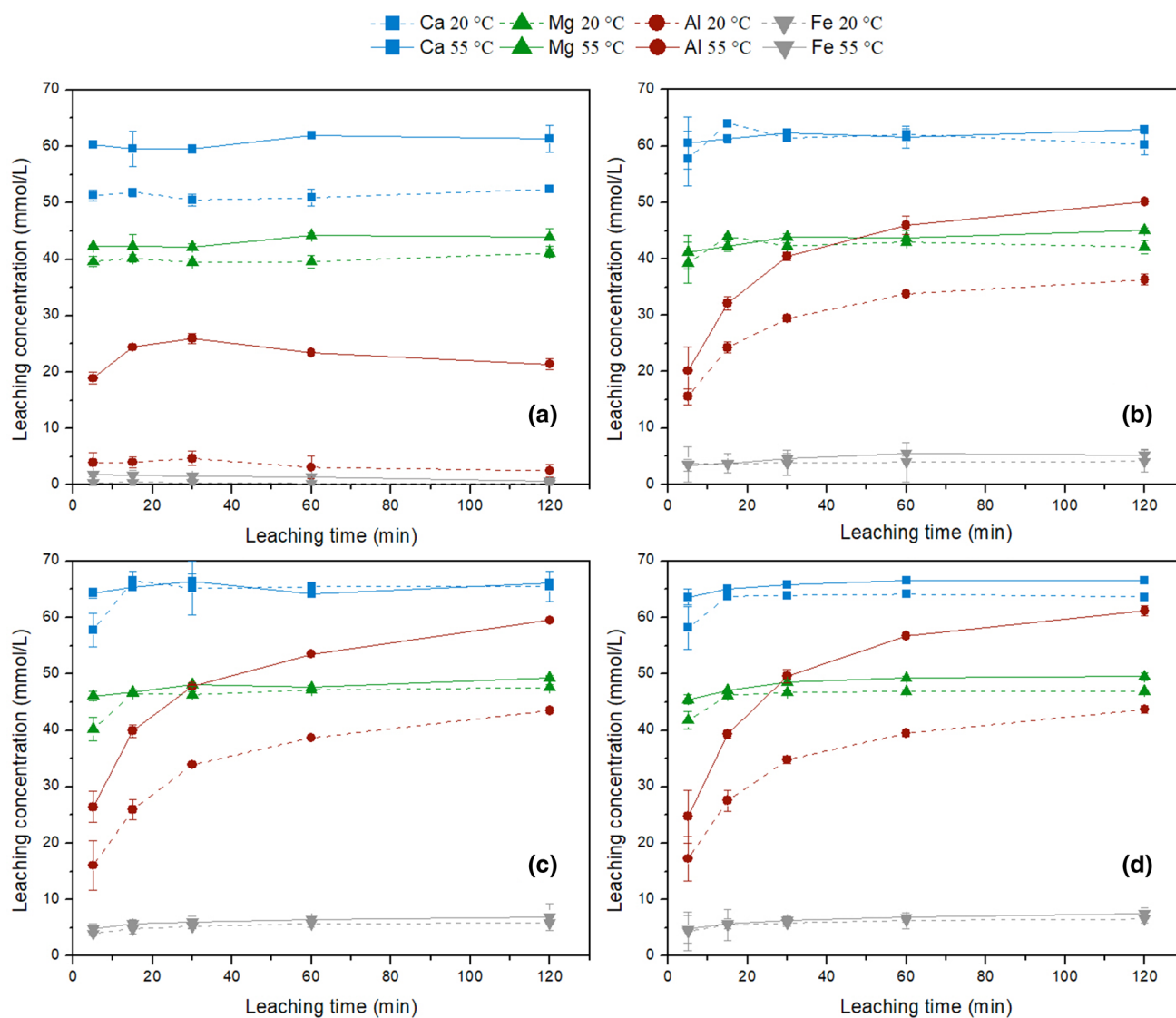
Fig. 4 Effects of acid concentration and time on metal leaching concentration (L/S = 20 L/kg). **a** HCl 0.2 mol/L; **b** HCl 0.3 mol/L; **c** HCl 0.4 mol/L; **d** HCl 0.5 mol/L

due after leaching at 55 °C and L/S = 20 L/kg for 15 min (time required to reach the maximum P leaching ratio) and 120 min (time required to reach the minimum P leaching ratio) using 0.2 mol/L HCl were analyzed and compared to determine the morphology and mass distribution transformation patterns during the P leaching process when the acid concentration was lower than the theoretical acid concentration. The results could help to optimize the leaching method and guide the product preparation technique.

As shown in Fig. S2, the main crystal phase SiO_2 existed in a stable manner in the solid residue after leaching. Basically, the iron-containing compounds did not dissolve. By contrast, $Mg_3Ca_3(PO_4)_4$ and $Ca_{2.7}Mg_{0.29}(PO_4)_2$ almost dissolved completely after leaching for 15 min using 0.2 mol/L HCl, and thus, their diffraction peaks disappeared. The

diffraction peak appeared for $Fe_4(OH)_3(PO_4)_3$. The XRD diffraction pattern clearly indicated the overlapping of multiple crystal phase peaks, such as those for $AlPO_4$ and SiO_2. Hence, deconvolution was required to distinguish the phases corresponding to the overlapping peaks and to determine the changes in the phase content.

Quantitative analysis of crystalline and amorphous phases Based on the qualitative analytical results for the crystal phases, Cr_2O_3 was added as an internal standard to analyze the absolute contents of each crystal phase and amorphous phase using the Rietveld refinement method. Figure S7–S9 shows the Rietveld refined XRD spectra for the ISSA and solid residues, respectively, where the cross spectrum (Obs) represents the test result, the red line spec-

trum (Calc) is the fitted result, and the blue line spectrum (Diff) is the difference between the fitted spectrum and the test spectrum. The short lines with different colors indicate the Bragg positions in the XRD spectra for each corresponding phase (the colors presented for each phase are the same as those in Fig. S2). The fitting factor Rwp was less than 5% and Rp was less than 4%. The fitting spectrum agreed well with the test spectrum. The quantitative results are shown in Table 4 and Fig. 5.

Figure 5 shows that $Mg_3Ca_3(PO_4)_4$ and $Ca_{2.7}Mg_{0.29}(PO_4)_2$ dissolved completely after leaching using 0.2 mol/L HCl, whereas the contents of $Fe_3(H_2O)_3(PO_4)_2$ and $Fe_4(OH)_3(PO_4)_3$ increased in the solid residue. Based on the absolute amount (component content multiplied by the solid mass) of each component before and after leaching, 44% of the $AlPO_4$ dissolved after leaching for 15 min, and after leaching for 120 min, the absolute amounts of $AlPO_4$, $Fe_3(H_2O)_3(PO_4)_2$, and $Fe_4(OH)_3(PO_4)_3$ in the solid residue increased by nearly 20.7%, 1.6%, and 83.3%, respectively. Therefore, the phosphorus in the forms of $Mg_3Ca_3(PO_4)_4$ and $Ca_{2.7}Mg_{0.29}(PO_4)_2$ dissolved rapidly, whereas that in the form of $AlPO_4$ dissolved partially in the early stage. When the acid concentration was insufficient (less than the theoretical acid concentration), phosphorus precipitated in the forms of $AlPO_4$, $Fe_3(H_2O)_3(PO_4)_2$, and $Fe_4(OH)_3(PO_4)_3$, and it was re-fixed in the solid phase as the leaching process continued.

Effects of pH on the phase dissolution equilibrium The solubility of phosphate is closely related to pH [46]. Visual Minteq 3.1 software was used to simulate the effects of pH on the dissolution equilibrium for elemental P (PO_4^{3-}), Ca, Mg, Al, and Fe. According to the simulation results (Fig. 6), Fe precipitated as $FePO_4·2H_2O$ at pH 0.6 and Al gradually precipitated as apatite ($AlPO_4·2H_2O$) at pH 1.4. Figure S10 shows the leaching concentrations of elemental P, Ca, Mg, Al, and Fe, and the pH over time at 55 °C using 0.2 mol/L HCl for leaching. As the reaction continued, the leachate pH gradually increased from 1.8 to 2.0, where the leaching ratios of P, Al, and Fe gradually decreased after leaching for 30 min, whereas those of Ca and Mg basically remained unchanged. Therefore, increasing the pH enhanced the combination of P with Al and Fe to transform into the solid phase [8]. The leaching concentrations of P, Al, and Fe decreased by 18.5 mmol/L, 4.5 mmol/L, and 1.0 mmol/L, respectively, from 15 to 120 min. As the pH increased, P, Al, and Fe dissolved initially and then combined to precipitate as $AlPO_4$, $Fe_3(H_2O)_3(PO_4)_2$, and $Fe_4(PO_4)_3(OH)_3$. In this case, the leached concentration of P decreased by 5.2 mmol/L based on stoichiometry, but this value did not agree with that obtained as 18.5 mmol/L, and thus part of the P probably combined with the subsequently dissolved Al to form the precipitate $AlPO_4$. When

Table 4 Contents of crystalline and amorphous phases in the ISSA and solid residues (%)

Samples	SiO_2	$Mg_3Ca_3(PO_4)_4$	$CaAl_2Si_2O_8$	$AlPO_4$	$Ca_{2.7}Mg_{0.29}(PO_4)_2$	Fe_2O_3	$Fe_{1.833}(OH)_{0.5}O_{2.5}$	$Fe_3(H_2O)_3(PO_4)_2$	$Fe_4(OH)_3(PO_4)_3$	Amorphous phases
ISSA	23.14	12.23	10.65	11.19	4.82	1.53	1.31	1.31	0	33.79
Solid residue (0.2 mol/L HCl, 15 min)	36.84	0	16.46	8.33	0	2.8	1.61	2.8	1.19	27.25
Solid residue (0.2 mol/L HCl, 120 min)	34.81	0	17.86	10.29	0	4.68	2.06	2.94	2.23	25.11

Fig. 5 Mass distribution of phosphorus compounds in ISSA and solid residues (55 °C, 0.2 mol/L HCl, L/S = 20 L/kg)
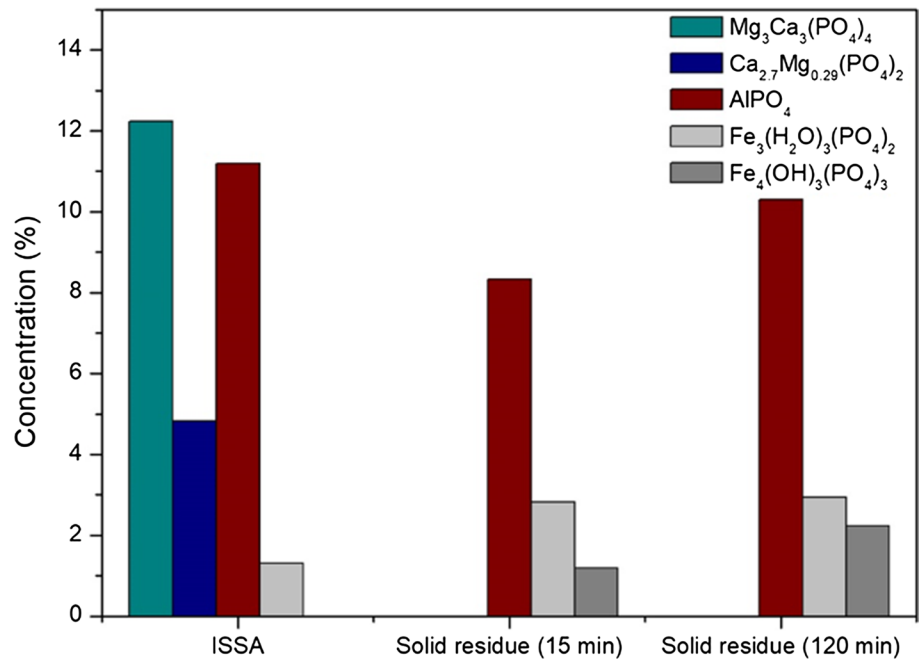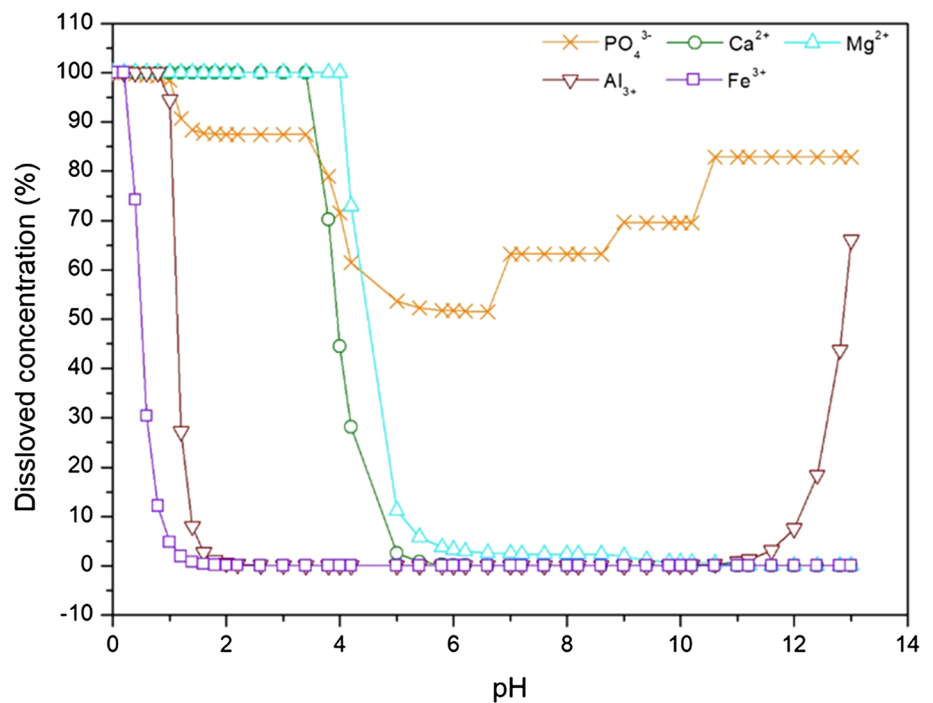

**Fig. 6** Effects of pH on the element dissolution equilibrium (55 °C)

the HCl concentration was 0.3 mol/L, the leached concentration of Al increased by about 18 mmol/L, thereby indicating that $AlPO_4$ re-dissolved and this confirmed the assumption above, i.e., immediate precipitation of P with newly dissolved Al at 0.2 mol/L HCl.

Surface micromorphology analysis

The surface morphologies of the solid samples are shown in Fig. 7. The irregular crystal surface of ISSA comprised many plate-like silica structures (Fig. 7a) with rough accumulation

Fig. 7 Surface micromorphology of ISSA and solid residue (L/S = 20 L/kg). **a** ISSA; **b** 55 °C 0.2 mol/L HCl, 15 min; **c** 55 °C 0.2 mol/L HCl, 120 min; **d** 55 °C 0.5 mol/L HCl, 60 min
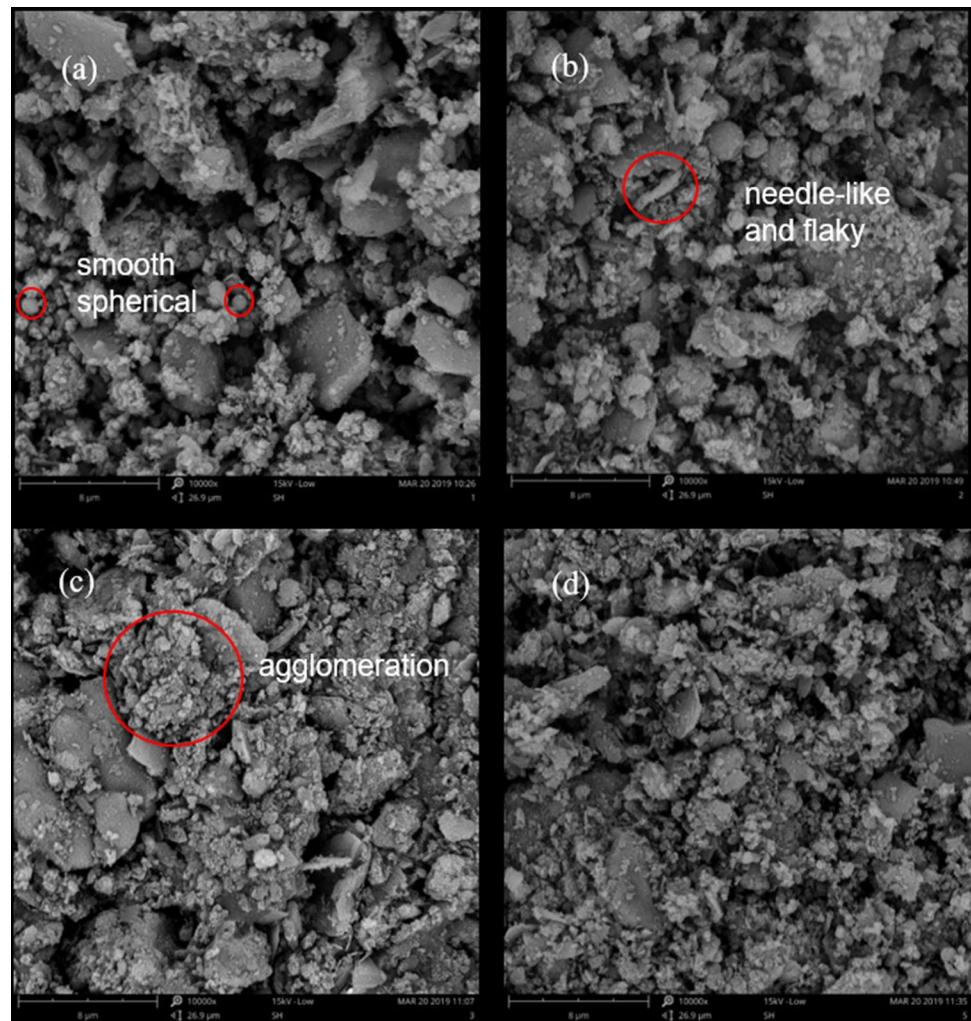
holes. In addition, clear agglomerations were observed and some particles had smooth surfaces with spherical morphology. After leaching for 15 min, the soluble salts dissolved on the surface of ISSA and the ISSA particles became smaller, where the surface was looser and more porous with needle-like and flaky structures. As the acid concentration increased, the agglomeration of large particles decreased and the amount of fine particles increased. Figure 7b, c shows that the plate-like structures in the solid residue after leaching for 120 min adsorbed more agglomerated particles, and thus, the particle size increased and the inter-particle spaces were smaller, which reflected the occurrence of re-precipitation and adsorption processes.

According to the EDX spectra obtained for the ISSA and solid residue (Fig. S11), elemental O, C, Si, Al, P, and Fe still remained in the solid residue after leaching for 120 min using 0.2 mol/L HCl, whereas elemental Ca and Mg were not detected. Thus, these results confirmed that the compounds in the form of Ca–Mg–P in the ISSA basically dissolved, whereas most of the compounds in the forms of Fe–P

and Al–P still remained in the solid residue. Ca, Mg, Fe, and P were not detected in the solid residues from 0.5 mol/L HCl leaching, indicating that all P-containing compounds dissolved, which is consistent with the leaching result.

Conclusions

1. Hydrochloric acid rapidly and effectively achieved the highly efficient leaching of P from ISSA. The P leaching ratio exceeded 80% when the temperature was 55 °C with a HCl concentration of 0.2–0.5 mol/L and after leaching for 15 min. The P leaching ratio increased initially and then decreased at 0.2 mol/L HCl. When the acid concentration increased to 0.5 mol/L, the P leaching ratio gradually increased to reach an equilibrium.

2. The Drozdov equation includes self-impeding factors and it was used to analyze the dynamic control factors of the leaching process. The model fitted well but especially for 0.2 mol/L HCl (the correlation coefficient was

approximately 1). The activation energy was obtained as 19.26 kJ/mol based on the reaction rate at different temperatures, thereby demonstrating that the leaching process from ISSA was controlled by factors comprising chemical reactions and diffusion. In addition, the re-precipitation of P-containing compounds hindered the reaction from proceeding rapidly as an obvious self-impeding effect.

3. The phosphorus leaching patterns were obtained according to qualitative and quantitative analyses of the ISSA and solid residues. Initially, $Mg_3Ca_3(PO_4)_4$ and $Ca_{2.7}Mg_{0.29}(PO_4)_2$ dissolved, while $AlPO_4$ partially dissolved as the pH increased, and P then precipitated in the forms of $AlPO_4$, $Fe_3(H_2O)_3(PO_4)_2$, and $Fe_4(OH)_3(PO_4)_3$, which were re-fixed in the solid residue.

References

1. Petzet S, Peplinski B, Cornel P. On wet chemical phosphorus recovery from sewage sludge ash by acidic or alkaline leaching and an optimized combination of both. Water Res. 2012;46(12):3769–80. https://doi.org/10.1016/j.watres.2012.03.068.

2. Jasinski SM. Minerals Yearbook: phosphate rock. Phosphate rock. U.S.Geological Survey; 2016.

3. Cordell D, Drangert J-O, White S. The story of phosphorus: Global food security and food for thought. Glob Environ Change. 2009;19(2):292–305. https://doi.org/10.1016/j.gloenvcha.2008.10.009.

4. Xue YG, Wu FF, Liu XJ, et al. A review on phosphorus recovery technology and Its application in the sewage sludge recycling. Environ Sci Technol. 2014;37(S2):247–51.

5. Smil V. Phosphorus in the environment: natural flows and human interferences. Annu Rev Energy Env. 2000;25(1):53–88. https://doi.org/10.1146/annurev.energy.25.1.53.

6. Franz M. Phosphate fertilizer from sewage sludge ash (SSA). Waste Manage. 2008;28(10):1809–18. https://doi.org/10.1016/j.wasman.2007.08.011.

7. Cornel P, Schaum C. Phosphorus recovery from wastewater: needs, technologies and costs. Water Sci Technol. 2009;59(6):1069–76. https://doi.org/10.2166/wst.2009.045.

8. Lim BH, Kim D-J. Selective acidic elution of Ca from sewage sludge ash for phosphorus recovery under pH control. J Ind Eng Chem. 2017;46:62–7. https://doi.org/10.1016/j.jiec.2016.10.016.

9. Herzel H, Kruger O, Hermann L, et al. Sewage sludge ash–A promising secondary phosphorus source for fertilizer production. Sci Total Environ. 2016;542(Pt B):1136–43. https://doi.org/10.1016/j.scitotenv.2015.08.059.

10. Chen T, Yan B. Fixation and partitioning of heavy metals in slag after incineration of sewage sludge. Waste Manage. 2012;32(5):957–64. https://doi.org/10.1016/j.wasman.2011.12.003.

11. Medici F, Piga L, Rinaldi G. Behaviour of polyaminophenolic additives in the granulation of lime and fly-ash. Waste Manage. 2000;20(7):491–8. https://doi.org/10.1016/S0956-053X(00)00030-1.

12. Pettersson A, Åmand L-E, Steenari B-M. Leaching of ashes from co-combustion of sewage sludge and wood—Part I: Recovery of phosphorus. Biomass Bioenerg. 2008;32(3):224–35. https://doi.org/10.1016/j.biombioe.2007.09.016.

13. Adam C, Peplinski B, Michaelis M, et al. Thermochemical treatment of sewage sludge ashes for phosphorus recovery. Waste Manage. 2009;29(3):1122–8. https://doi.org/10.1016/j.wasman.2008.09.011.

14. Lee M, Kim D-J. Identification of phosphorus forms in sewage sludge ash during acid pre-treatment for phosphorus recovery by chemical fractionation and spectroscopy. J Ind Eng Chem. 2017;51:64–70. https://doi.org/10.1016/j.jiec.2017.02.013.

15. Fang L, Li JS, Guo MZ, et al. Phosphorus recovery and leaching of trace elements from incinerated sewage sludge ash (ISSA). Chemosphere. 2018;193:278–87. https://doi.org/10.1016/j.chemosphere.2017.11.023.

16. Kalmykova Y, Karlfeldt FK. Phosphorus recovery from municipal solid waste incineration fly ash. Waste Manage. 2013;33(6):1403–10. https://doi.org/10.1016/j.wasman.2013.01.040.

17. Li J-S, Chen Z, Wang Q-M, et al. Change in re-use value of incinerated sewage sludge ash due to chemical extraction of phosphorus. Waste Manage. 2018;74:404–12. https://doi.org/10.1016/j.wasman.2018.01.007.

18. Biswas BK, Inoue K, Harada H, et al. Leaching of phosphorus from incinerated sewage sludge ash by means of acid extraction followed by adsorption on orange waste gel. J Environ Sci. 2009;21(12):1753–60. https://doi.org/10.1016/S1001-0742(08)62484-5.

19. Ottosen LM, Kirkelund GM, Jensen PE. Extracting phosphorous from incinerated sewage sludge ash rich in iron or aluminum. Chemosphere. 2013;91(7):963–9. https://doi.org/10.1016/j.chemosphere.2013.01.101.

20. Falayi T. Alkaline recovery of phosphorous from sewage sludge and stabilisation of sewage sludge residue. Waste Manage. 2019;84:166–72. https://doi.org/10.1016/j.wasman.2018.11.041.

21. Meng X, Liu X, Huang Q, et al. Recovery of phosphate as struvite from low-temperature combustion sewage sludge ash (LTCA) by cation exchange. Waste Manage. 2019;90:84–93. https://doi.org/10.1016/j.wasman.2019.04.045.

22. Wang Q, Li J-S, Tang P, et al. Sustainable reclamation of phosphorus from incinerated sewage sludge ash as value-added struvite by chemical extraction, purification and crystallization. J Clean Prod. 2018;181:717–25. https://doi.org/10.1016/j.jclepro.2018.01.254.

23. Xu H, He P, Gu W, et al. Recovery of phosphorus as struvite from sewage sludge ash. J Environ Sci. 2012;24(8):1533–8. https://doi.org/10.1016/S1001-0742(11)60969-8.

24. Donatello S, Tong D, Cheeseman CR. Production of technical grade phosphoric acid from incinerator sewage sludge ash (ISSA). Waste Manage. 2010;30(8–9):1634–42. https://doi.org/10.1016/j.wasman.2010.04.009.

25. Li R, Zhang Z, Li Y, et al. Transformation of apatite phosphorus and non-apatite inorganic phosphorus during incineration of sewage sludge. Chemosphere. 2015;141:57–61. https://doi.org/10.1016/j.chemosphere.2015.05.094.

26. Shiba NC, Ntuli F. Extraction and precipitation of phosphorus from sewage sludge. Waste Manage. 2017;60:191–200. https://doi.org/10.1016/j.wasman.2016.07.031.

27. Yang F, Chen J, Yang M, et al. Phosphorus recovery from sewage sludge via incineration with chlorine-based additives. Waste Manage. 2019;95:644–51. https://doi.org/10.1016/j.wasman.2019.06.029.

28. Vogel C, Adam C. Heavy metal removal from sewage sludge ash by thermochemical treatment with gaseous hydrochloric acid. Environ Sci Technol. 2011;45(17):7445–500. https://doi.org/10.1021/es2007319.

29. Krüger O, Adam C. Phosphorus in recycling fertilizers - analytical challenges. Environ Res. 2017;155:353–8. https://doi.org/10.1016/j.envres.2017.02.034.

30. Winburn R, Grier D, Mccarthy GJ, et al. Rietveld quantitative X-ray diffraction analysis of NIST fly ash standard reference materials. Powder Diffr. 2000;15(3):163–72. https://doi.org/10.1017/S0885715600011015.

31. Gualtieri A. Modal analysis of piroclastic rocks by combined rietveld and RIR methods. Powder Diffr. 1996;11(2):97–106. https://doi.org/10.1017/S0885715600009052.

32. (Mep) MOEP. Solid waste-determination of 22 metal elements—inductively couples plasma optical emission spectrometry. Beijing: China Environmental Science Press; 2016.

33. Gualtieri ML, Prudenziati M, Gualtieri AF. Quantitative determination of the amorphous phase in plasma sprayed alumina coatings using the Rietveld method. Surf Coat Technol. 2006;201(6):2984–9. https://doi.org/10.1016/j.surfcoat.2006.06.009.

34. Kim W, Zhang Q, Saito F. Mechanochemical synthesis of hydroxyapatite from $Ca(OH)_2$–P_2O_5 and $CaO\text{-}Ca(OH)_2$–P_2O_5 mixtures. J Mater Sci. 2000;35(21):5401–5. https://doi.org/10.1023/a:1004859231795.

35. Hoffmann G, Schingnitz D, Bilitewski B. Comparing different methods of analysing sewage sludge, dewatered sewage sludge and sewage sludge ash. Desalination. 2010;250(1):399–403. https://doi.org/10.1016/j.desal.2009.09.064.

36. Budhathoki R, Väisänen A, Lahtinen M. Selective recovery of phosphorus as $AlPO_4$ from silicon-free CFB-derived fly ash leachate. Hydrometallurgy. 2018;178:30–6. https://doi.org/10.1016/j.hydromet.2018.03.025.

37. Li X, Xing P, Du X, et al. Influencing factors and kinetics analysis on the leaching of iron from boron carbide waste-scrap with ultrasound-assisted method. Ultrason Sonochem. 2017;38:84–91. https://doi.org/10.1016/j.ultsonch.2017.02.037.

38. Maccarthy J, Nosrati A, Skinner W, et al. Acid leaching and rheological behaviour of a siliceous goethitic nickel laterite ore: Influence of particle size and temperature. Miner Eng. 2015;77:52–63. https://doi.org/10.1016/j.mineng.2014.12.031.

39. Hosseini SA, Raygan S, Rezaei A, et al. Leaching of nickel from a secondary source by sulfuric acid. J Environ Chem Eng. 2017;5(4):3922–9. https://doi.org/10.1016/j.jece.2017.07.059.

40. Fang L, Li J-S, Donatello S, et al. Recovery of phosphorus from incinerated sewage sludge ash by combined two-step extraction and selective precipitation. Chem Eng J. 2018;348:74–83. https://doi.org/10.1016/j.cej.2018.04.201.

41. Liu DJ, Zhong BH, Zhang YX. Liquid and solid phase reaction kinetics of phosphoric acid complex system (II) experimental study on digestion kinetics of phosphate ore particle system. CIESC J. 2001;01:28–34.

42. Papamichael EM, Economou ED, Vaimakis TC. Dissolution of the carbonate minerals of phosphate ores: catalysis by carbonic anhydrase II, from bovine erythrocytes, in acid solutions. J Colloid Interface Sci. 2002;251(1):143–50. https://doi.org/10.1006/jcis.2002.8366.

43. Economou ED, Vaimakis TC, Papamichael EM. The kinetics of dissolution of the carbonate minerals of phosphate ores using dilute acetic acid solutions: the case of pH range from 3.96 to 6.40. J Colloid Interface Sci. 2002;245(1):133–41. https://doi.org/10.1006/jcis.2001.7931.

44. Li M, Wei C, Qiu S, et al. Kinetics of vanadium dissolution from black shale in pressure acid leaching. Hydrometallurgy. 2010;104(2):193–200. https://doi.org/10.1016/j.hydromet.2010.06.001.

45. Dickinson CF, Heal GR. Solid-liquid diffusion controlled rate equations. Thermochim Acta. 1999;340–341:89–103. https://doi.org/10.1016/S0040-6031(99)00256-7.

46. Tanada S, Kabayama M, Kawasaki N, et al. Removal of phosphate by aluminum oxide hydroxide. J Colloid Interface Sci. 2003;257(1):135–40. https://doi.org/10.1016/S0021-9797(02)00008-5.